

# Calcification state of coccolithophores can be assessed by light scatter depolarization measurements with flow cytometry

PETER VON DASSOW<sup>1\*</sup>, GER VAN DEN ENGH<sup>2</sup>, DEBORA IGLESIAS-RODRIGUEZ<sup>3</sup> AND JOHN R. GITTINS<sup>3</sup>

<sup>1</sup>DEPARTAMENTO DE ECOLOGÍA, FACULTAD DE CIENCIAS BIOLÓGICAS, PONTIFICIA UNIVERSIDAD CATÓLICA DE CHILE AVENIDA BERNADO O'HIGGINS 340, EDIFICIO 210, SANTIAGO, CHILE, <sup>2</sup>BD ADVANCED CYTOMETRY GROUP, BD BIOSCIENCES, SEATTLE, WA, USA AND <sup>3</sup>OCEAN BIOGEOCHEMISTRY AND ECOSYSTEMS, NATIONAL OCEANOGRAPHY CENTRE, SOUTHAMPTON, UK

\*CORRESPONDING AUTHOR: pvondassow@bio.puc.cl, pvondass@gmail.com

Received March 2, 2012; accepted August 16, 2012

Corresponding editor: John Dolan

Coccolithophores are important primary producers and a dominant group of calcifying organisms in the ocean. Calcification state depends on genetic, physiological and environmental factors. We show that flow cytometric measurement of the depolarization forward scattered light using a Brewster's Window Analyzer can be used to quantify the degree of calcification of coccolithophores at the single-cell level. Calcite-containing particles or cells were distinguished from non-calcified particles or cells by high values of forward scatter light with polarization orthogonal to that of the laser. Forward scatter polarization state varied strongly and linearly with the number of attached coccoliths per coccosphere when *Emiliania huxleyi* cells were first completely decalcified and then allowed to rebuild coccospheres. Cells of the heavily calcified *E. huxleyi* R-morphotype strain NZEH were also grown in different extracellular  $\text{Ca}^{2+}$  concentrations, forming complete coccospheres that contained similar numbers of attached coccoliths but varied in total calcite mass. Forward scatter polarization state varied strongly and linearly with coccosphere calcite mass. In contrast, forward scatter polarization state of detached coccoliths did not vary significantly with calcite weight, although forward scatter and side scatter did. Treatments had relatively minor effects on forward scatter, side scatter and forward scatter polarization state of decalcified cells, suggesting that depolarization of forward scatter light from *E. huxleyi* cells might be linearly determined, to a first approximation, by the ratio of surface calcite to organic protoplast. We suggest that flow cytometric measurement of forward scatter depolarization provides a potentially valuable method for analysis of calcification state of individual cells.

**KEYWORDS:** flow cytometry; light polarization; coccolithophore; calcification; phytoplankton

## INTRODUCTION

Coccolithophores are important in the carbon chemistry of the ocean, as they are the dominant producers of particulate inorganic carbon, in the form of extracellular calcium carbonate coccoliths. Calcification results in the net conversion of two  $\text{HCO}_3^-$  ions into one molecule of  $\text{CO}_2$  and one molecular unit of  $\text{CaCO}_3$ , so it represents an immediate source of  $\text{CO}_2$  (Frankignoulle *et al.*, 1994; Berry *et al.*, 2002) and the net effect of coccolithophores on ocean carbon chemistry (as a source or a sink for dissolved  $\text{CO}_2$  gas in the water column) depends on the ratio of calcification to photosynthesis (Zondervan, 2007). Calcite coccoliths might also increase carbon export from surface layers by increasing the sinking rate of particles (Armstrong *et al.*, 2001; Ziveri *et al.*, 2007). The role of calcification by coccolithophores varies with their abundance and according to genetic and physiological factors controlling calcification state. Ocean acidification resulting from increases in atmospheric  $\text{pCO}_2$  is expected to affect the calcification of marine plankton and the ocean carbonate system (Feely *et al.*, 2004; Feng *et al.*, 2009). Laboratory experiments investigating ocean acidification impacts on coccolithophores using cultured species have yielded variable results, with the observation of increases, decreases, neutral and non-uniform calcification responses (Riebesell *et al.*, 2000; Langer *et al.*, 2006; Zondervan, 2007; Feng *et al.*, 2008; Iglesias-Rodriguez *et al.*, 2008). Opposite effects of simulated ocean acidification have been observed among different strains of *Emiliania huxleyi* even in the same laboratory environment (Langer *et al.*, 2009). In addition, greatly differing calcification states can typify neighboring populations observed in nature (Beaufort *et al.*, 2008, 2011). These observations suggest that the effects of ocean acidification on planktonic calcification might vary greatly between environments depending partly on dominant genotypes and environmental variables, emphasizing the importance of observing changes in the proportions of calcified cells and their calcification state in a variety of environments.

Measurements of phytoplankton calcification are traditionally made by collecting a water sample on a filter and calculating the concentration of particulate inorganic carbon as the difference between total carbon before and after acidification to dissolve calcium carbonate (Ehrhardt and Koeve, 2007). Optical methods to measure backscattering from acid-labile birefringent particles have also been applied to whole water samples to detect particulate inorganic carbon (Balch *et al.*, 2001). However, both calcifying and non-calcifying species co-occur in nature and, within a calcifying

species, both calcified and non-calcified forms can be present (Klaveness and Paasche, 1971). Likewise, calcite-containing particles include both living cells covered in coccoliths, empty coccospheres and detached coccoliths. Determining the contributions of different particle types to bulk particulate carbon fractions traditionally involves intensive microscopic counting and identification, combined with estimates of the organic and inorganic carbon associated with each cell from values obtained in culture on representative species. The development of an automated polarized light microscope has been a great advance, permitting direct estimates of the calcite on individual coccoliths and coccospheres (Beaufort *et al.*, 2008), but techniques for rapidly characterizing both calcified and non-calcified particles in phytoplankton samples are still needed.

Flow cytometers using polarizing filters to determine the polarization state of forward scattered laser light have been shown to be able to discriminate calcified particles, which change light scatter polarization presumably due to the birefringence of calcite (Olson *et al.*, 1989; Balch *et al.*, 1999), but it has yet to be shown whether this technique can accurately quantify calcite levels on single cells. We tested a new Brewster's Window Analyzer, which relies on the principle that the polarization of incident light determines how it is reflected or transmitted through a transparent surface (Lakhtakia, 1989), for analyzing the degree of forward scatter depolarization of single particles by cytometry. We focused specifically on *E. huxleyi*, as this species is the most numerically dominant coccolithophore in most regions of the modern ocean (Paasche, 2001), often occurring in concentrations  $>10^2$  cells  $\text{mL}^{-1}$  and capable of forming dense surface blooms with concentrations  $>10^3$  cells  $\text{mL}^{-1}$ . The principal objective of this study was to determine whether forward scatter polarization relates quantitatively to the amount of calcite on individual *E. huxleyi* cells. Our findings suggest that this technique might facilitate monitoring the calcification state of coccolithophores in laboratory experiments and in nature.

## METHOD

### Cultures and growth conditions

*Emiliania huxleyi* strains NZEH (heavily calcified), 61-12-04 (moderately calcified), CCMP1516 (weakly calcified) and CCMP2090 (non-calcified) were obtained from the Plymouth Culture Collection of Marine Microalgae and grown in f/4-Si medium using natural seawater or artificial seawater based on the Aquil recipe (Morel *et al.*, 1979) in which  $[\text{CaCl}_2]$  was varied.

Phosphate levels were reduced 6-fold in cultures of CCMP1516 and 61-12-04 to promote calcification. *Thalassiosira pseudonana* CCMP1335 was obtained from the Provasoli-Guillard National Center for the Culture of Marine Phytoplankton and grown in f/4. Cultures were grown at 20°C in 24 h light, 100  $\mu\text{mol photons m}^{-2} \text{s}^{-1}$ .

### Cell fixation

Cells were fixed by addition of 0.1 volumes of 100 mM sodium borate pH 8.7 solution containing 10% formaldehyde and 0.5% glutaraldehyde. Paraformaldehyde was dissolved in 100 mM sodium borate buffer at 65–70°C, subsequently filtered through Whatman paper filters, then the pH checked, and then glutaraldehyde was added before sterile 0.2  $\mu\text{m}$  filtration. The fixative was stored frozen in aliquots and thawed immediately prior to use. After addition of the fixative, samples were incubated in the dark for 15–20 min, flash-frozen in liquid nitrogen and stored at  $-20^\circ\text{C}$ .

### Non-living optical particles

Two and 6  $\mu\text{m}$  FlowCheck high-intensity yellow–green fluorescent calibration beads were obtained from Polysciences (#23518–10 and #23519–10, Polysciences, Warrington, PA, USA). Three-micrometer UltraRainbow beads were obtained from SpheroTech (Lake Forest, IL, USA). Calcite “Icelandic Spar” and limestone chalk (cliffs of Dover, UK), obtained from Edmunds Scientific (Tonawanda, NY, USA) were crushed, suspended in 10 mM  $\text{Na}_2\text{CO}_3$ , pH 9.0 and filtered through a 10  $\mu\text{m}$  filter.

### Light microscopy

Daily cell counts were performed using a Neubauer Haemocytometer and a Nikon Labophot2 upright microscope with 10 $\times$  and 40 $\times$  phase-contrast objectives. Cell imaging was performed with a 60 $\times$  oil immersion objective on a Nikon Eclipse 80i upright microscope (Nikon, Tokyo, Japan) equipped with differential interference contrast and a MicroPublisher 3.3 RTV color CCD camera (QImaging, Burnaby, BC, Canada). Images taken at three separate focal planes were used to count the number of attached coccoliths per cell. A minimum of 20 cells was analyzed per sample to determine attached coccoliths per cell (a 55 cell minimum was used for live cells). Cells were not included in counts if they did not appear intact and well pigmented. When more than one cell was included in a set of

images at three focal planes, all cells were counted when in similar focal depths.

### Scanning electron microscopy

Sample aliquots of 100–200  $\mu\text{L}$  were vacuum filtered onto 0.4  $\mu\text{m}$  polycarbonate membranes and rinsed with water alkalized with  $\text{NH}_4\text{OH}$  (pH  $\approx$  9) to rinse away seawater salts. Filter membranes were then dried, gold coated (using a Hummer VI-A sputter coater) and imaged using an 840ALEO 1450VP scanning electron microscope.

### Calcite analysis

Coccolithophore cultures were filtered onto 0.2  $\mu\text{m}$  polycarbonate filters, washed with alkalized water and dried. The filters were treated with 0.4 M  $\text{HNO}_3$  (Romil UpA grade) overnight to dissolve the  $\text{CaCO}_3$  coccoliths. The resulting solutions were filtered through 0.45  $\mu\text{m}$  hydrophilic PTFE membranes and analyzed using a Perkin Elmer Optima 4300 DV inductively coupled plasma-optical emission spectrometer calibrated against standard solutions bracketing the range of concentrations measured. Sodium concentrations were determined as a proxy for seawater contamination.

The amount of calcite (i.e. particulate inorganic carbon) attached to coccospheres was calculated as cellular particulate calcium ( $\text{PCa}_{\text{cell}}$ ):

$$\text{PCa}_{\text{cell}} = \text{PCa}_{\text{total}} \times \left( \frac{\text{attached coccoliths/cell}}{\text{attached coccoliths/cell} + \text{detached coccoliths/cell}} \right)$$

It was assumed that attached and detached coccoliths were similar in weight.

### Particulate organic carbon analysis

Samples for particulate organic carbon (POC) were filtered onto pre-combusted 25 mm GF/F filters. Inorganic carbonates were removed by acidification of the filters for 48 h with sulphurous acid under vacuum. The filters were dried at 60°C for 24 h, packaged in pre-combusted aluminum foil and analyzed with a Thermo Finnigan flash EA1112 elemental analyzer using acetanilide as the calibration standard.

### Flow cytometry

Light scatter and fluorescence measurements were made using an InFlux Cell Sorter cytometer (Cytopeia, Seattle,

WA, USA) equipped with a 488 nm laser. Laser polarization was normally vertical (parallel to the sample flow stream), but could be rotated using a half-wave plate placed in the laser beam. The polarization of forward scattered light was analyzed with two sequential glass plates forming Brewster's Windows incorporated into the Small Particle Detector option on the InFlux machine. A beam of linearly polarized light incident at Brewster's angle ( $\theta_B \approx 56^\circ$ ) to a glass surface is completely reflected if the plane of polarization is orthogonal to the plane of incidence but is completely transmitted if parallel to the plane of incidence (Fig. 1). The Brewster Window 1 was oriented so that forward scattered light had an angle of incidence of  $\theta_B$  in the vertical plane, transmitting forward scatter light with polarization parallel to the sample stream (parallel polarized forward scatter light; PFSC) and reflecting forward scatter light polarized orthogonal to the sample stream (orthogonally polarized forward scatter light; OFSC) to a photomultiplier (PMT) detector. The second Brewster Window, at  $\theta_B$  with respect to the horizontal plane, reflected forward scatter

light with polarization parallel to the sample stream (PFSC) to a second PMT detector. A neutral density filter was placed in the detector in the PFSC position to prevent light saturation. Other PMT detectors recorded side-scatter (SSC) and fluorescence emission at 530 nm (40 nm band pass), 580 nm (30 nm bandpass) and 692 nm (40 nm bandpass). Data from the fluorescence detector were amplified on a linear scale to more sensitively measure DNA fluorescence of stained cells. Laser alignment was checked with 2  $\mu\text{m}$  FlowCheck beads and the coefficient of variation (CV) in the 530 nm signal and FSC signals was always  $\approx 2\%$ . Fine-tuning of Brewster Windows was performed once optimal laser alignment had been achieved. First, the polarization of the laser beam was rotated to the horizontal position (orthogonal to the sample stream) by rotating the half-wave plate  $90^\circ$ . Slight adjustments were made to the first Brewster plate to maximize the scatter signal received by the OFSC detector. The laser polarization was then rotated back parallel to the sample stream and slight adjustments to the second Brewster plate were then

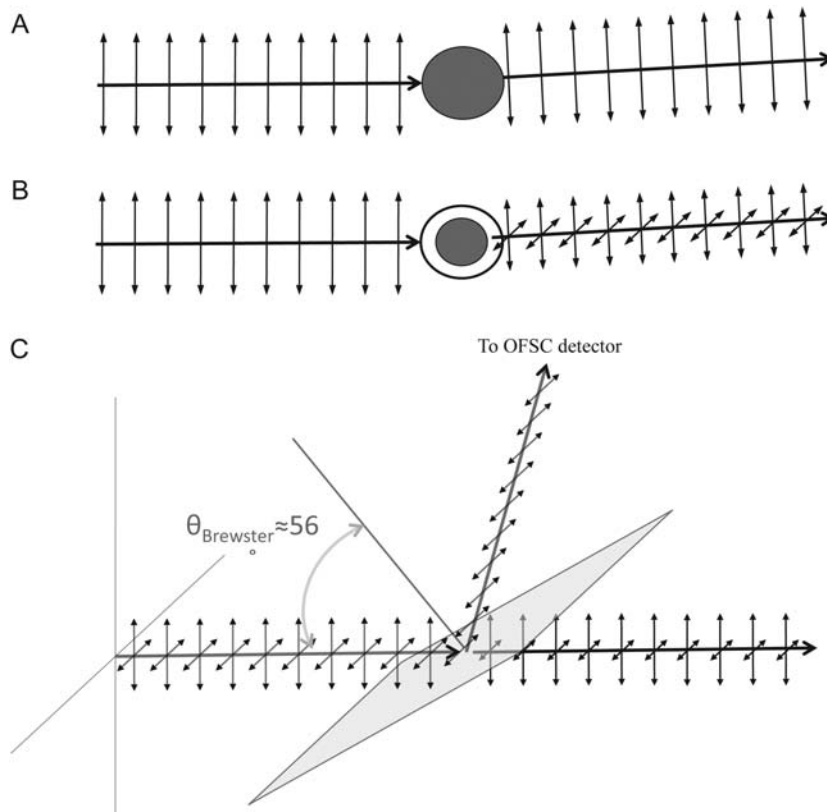


**Fig. 1.** Use of Brewster angle optics to measure depolarization of forward scatter light by cells and particles. **(A)** Laser light is polarized (parallel to sample stream) and light polarization is maintained when scattered off of a particle with low optical activity. **(B)** Laser light is partially depolarized when scattered off of a particle with high optical activity (e.g. a cell encased in a coccosphere). **(C)** A glass window placed at Brewster's angle reflected light with a polarization orthogonal to the original polarization, but light that maintains the original polarization is 100% transmitted. Some orthogonally polarized light is transmitted by the first Brewster's Window, so transmitted light is next analyzed by a second Brewster's Window (not shown), oriented to reflect only parallel polarized light.

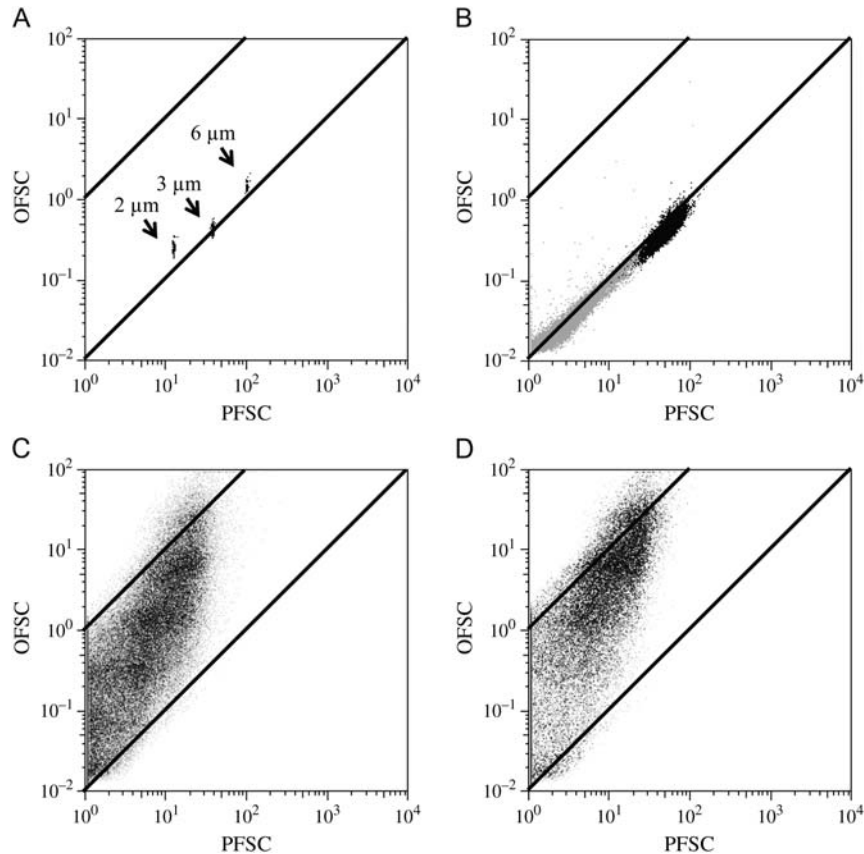


**Fig. 2.** Flow cytometric plots of OFSC versus PFSC for a variety of non-calcifying and calcifying particles. **(A)** A mix of 2 and 6  $\mu\text{m}$  FlowCheck beads and 3  $\mu\text{m}$  UltraRainbow beads. **(B)** The diatom *T. pseudonana* CCMP1335. Contour plot (of chlorophyll-containing cells) overlaid on shaded density plot of non-fluorescent particles (cell debris and media precipitates). **(C)** Crushed calcite crystal. **(D)** Crushed chalk. In all plots, the upper diagonal lines represent OFSC to PFSC ratios of 1:1 and 1:100, respectively.

made to maximize the scatter signal received by the PFSC detector. The OFSC and PFSC detector voltages were then adjusted so that particles with weak or no polarizing effect fell near a 1:1 line on a plot of OFSC versus PFSC signal.

Quantitative investigation of the relationship between calcification state and the polarization of forward scattered light required inter-calibration of the PMT detectors in the OFSC and PFSC positions by exchanging the two PMTs without altering the detector voltages or cytometer optics. The signal from 3  $\mu\text{m}$  UltraRainbow fluorescent beads on PMT#1 increased 88-fold when the PMT#1 was moved from the OFSC to PFSC position, while the signal on the PMT#2 decreased 88-fold when moved in the opposite direction. Gains were set so that the signal from PMT#1 in the OFSC position equaled the signal from PMT#2 in the PFSC position when 3  $\mu\text{m}$  UltraRainbow beads were analyzed, signifying that PMT#1 was set to an absolute photon sensitivity 88-fold greater than PMT#2.

The polarization of a light ray passing through a single calcite crystal may be rotated, rather than

depolarized, whereas a ray passing through many crystals of different orientations may be depolarized. For simplicity, we refer to a high OFSC/PFSC ratio as depolarization.

Flow cytometry analyses were performed using the program FlowJo 8.8.6 (Ashland, OR, USA).

### Statistical analysis

Linear regressions, analyses of variance and Tukey's *post hoc* test were performed using Prism version 5.0b for Macintosh (Graphpad Software, La Jolla, CA, USA).

## RESULTS

The two detectors of the Brewster's Window analyzer were inter-calibrated (see the Method section), allowing us to measure quantitatively the ratio of orthogonally polarized forward scattered light (OFSC) to parallel polarized forward scattered light (PFSC). Fluorescent calibration beads showed an OFSC/PFSC ratio of

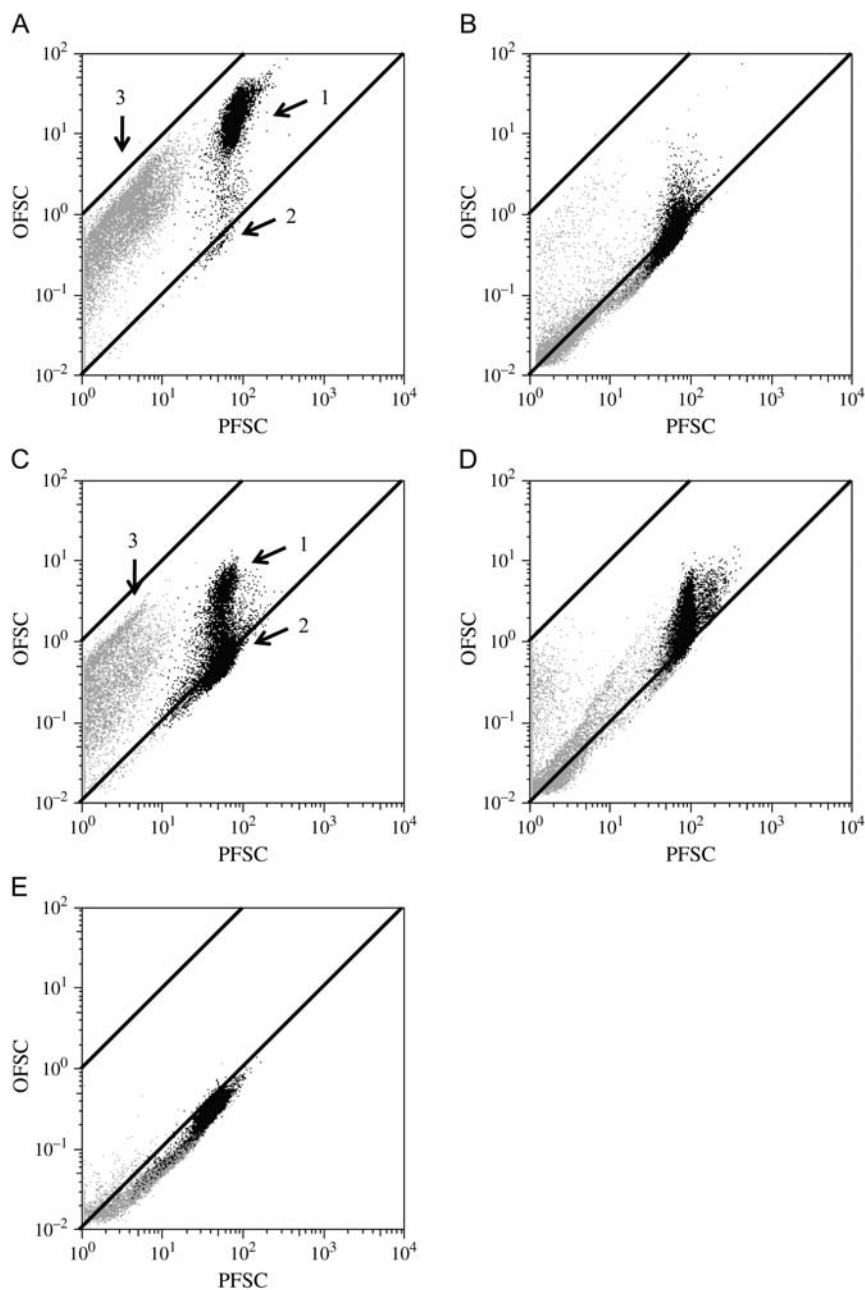


**Fig. 3.** Flow cytometric plots of OFSC versus PFSC for different strains of *E. huxleyi*. Dot plots representing chlorophyll-containing particles (*E. huxleyi* cells; dark gray) are overlaid on dot plots representing non-chlorophyll-containing particles (detached coccoliths, co-occurring bacteria, cell debris, media precipitate; light gray). For clarity,  $10^4$  particles of each particle class (chlorophyll-containing cells and non-chlorophyll-containing particles) are shown, to allow illustration of how particle properties vary. **(A)** Strain NZEH. Chlorophyll-containing coccospheres (1), chlorophyll-containing cells without calcite (2), and detached coccoliths (3) are indicated. Non-chlorophyll-containing particles represented 97.0% of the total particles analyzed. **(B)** The same NZEH sample after acidification. Note the drop in OFSC of chlorophyll-containing cells and the disappearance of de-attached coccoliths, which were the dominant non-fluorescent particle type in the non-acidified sample. After acidification, non-chlorophyll-containing particles represented only 28.6% of all particles analyzed, indicating that the majority of non-phytoplankton particles were acid-labile detached coccoliths (the rest represent cell debris, co-occurring bacteria, and non-acid-labile precipitates). Note that in both **(A)** and **(B)**, a total of  $10^4$  non-chlorophyll-containing particles are displayed. Despite the drop in total concentration between **(A)** and **(B)** following acidification, there is an apparent increase in the concentration of non-chlorophyll containing particles that do not display OFSC:PFSC ratios higher than 1:100. This is due in part to the fact that only  $10^4$  total non-chlorophyll-containing particles are displayed (causing a relative increase in the number of non-chlorophyll-containing particles with low OFSC when high OFSC-particles are dissolved by acidification) and in part to a real increase of  $\approx 2\times$  of non-chlorophyll-containing particles with low OFSC:PFSC ratios occurring likely due to release of organic particles adhered to detached coccoliths, generation of increased cell debris by mechanical effects of stirring during acidification and the acid-resistant organic casing found under coccospheres on some cells (Klavness and Paasche, 1971) and possibly organic remnants of dissolved coccoliths (see Supplementary data, Fig. S6 for more detail). **(C)** Moderately calcified strain 61-12-04. **(D)** Very weakly calcified strain CCMP1516. **(E)** Non-calcified strain CCMP2090.

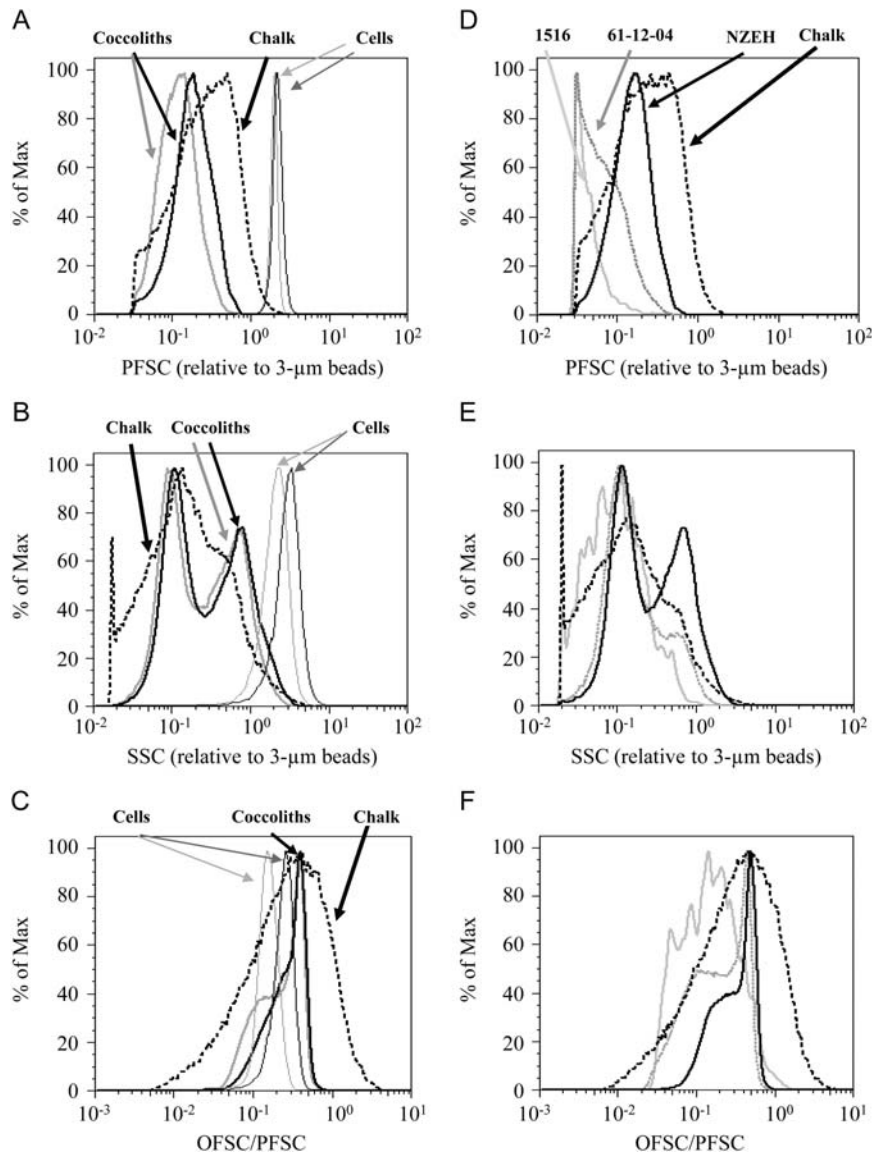


**Fig. 4.** Histograms of PFSC (**A** and **D**), SSC (**B** and **E**), and OFSC/PFSC (**C** and **F**) for chalk, *E. huxleyi* cells, and detached *E. huxleyi* coccoliths. (**A–C**) Histograms of chalk (thick dashed line), *E. huxleyi* cells (thin solid lines) and detached coccoliths (thick solid lines) grown at 12.5 (gray lines) and 150 (black lines)  $\mu\text{mole photon m}^{-2} \text{s}^{-1}$ . (**D–F**) Histograms of chalk (thick dashed lines), and detached coccoliths from heavily calcified strain NZEH (thick black lines), moderately calcified strain 61-12-04 (dark gray lines) and very weakly calcified strain CCMP1516 (light gray lines). Note that in these and subsequent figures, PFSC and SSC have been normalized by the geometric mean values for 3  $\mu\text{m}$  Ultrarainbow fluorescent beads.

$\approx 1\text{--}2\%$  (Fig. 2A). Likewise, non-calcified biological particles (diatom cells, non-calcified coccolithophores, bacteria and non-cellular debris co-occurring in phytoplankton cultures), displayed OFSC/PFSC ratios of  $\leq 0.01$  (Fig. 2B).

Calcified particles were characterized by increased OFSC relative to PFSC. Crushed calcite crystal particles (Fig. 2C) and crushed chalk (Fig. 2D) exhibited a broad distribution of OFSC relative to PFSC. The minimum OFSC/PFSC was similar to that of non-calcified

particles ( $\leq 0.01$ ) and the maximum OFSC/PFSC was over 1. However, the median OFSC signal increased faster than PFSC, indicating that the effect of calcite on forward scattered light polarization increased strongly with particle size and a small number of calcite crystals showed OFSC/PFSC ratios higher than 1 (consistent with partial rotation rather than complete depolarization of scattered light). Although chalk and calcite particles exhibited highly overlapping histograms of PFSC and SSC, calcite chalk exhibited a higher OFSC/PFSC,

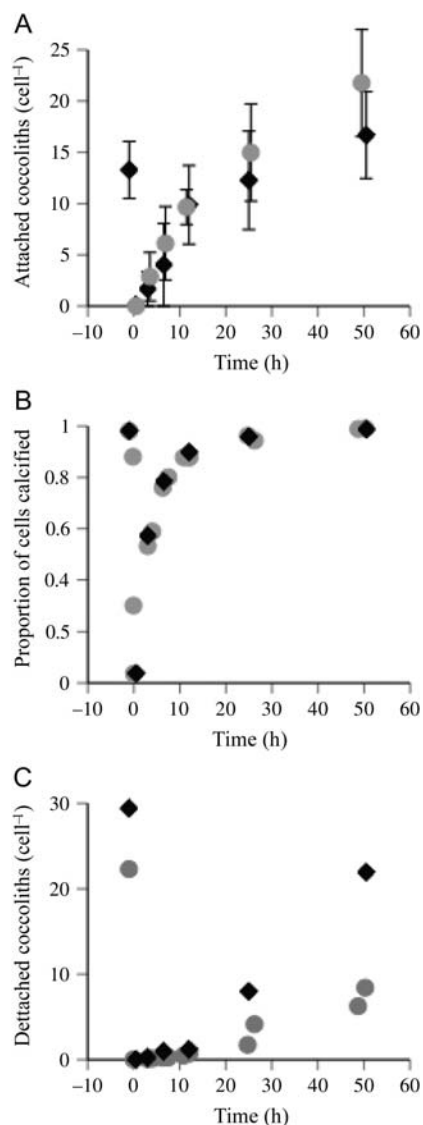


**Fig. 5.** Re-synthesis of coccoliths following acidification. **(A)** Attached coccoliths per cell (mean  $\pm$  standard deviation). **(B)** Proportion of chlorophyll-containing cells calcified. For clarity, error bars are not shown (coefficient of variation between duplicate fixed samples: mean 3.0%, range: 0.2–6.5%). **(C)** Detached coccoliths present in media per chlorophyll-containing cell. Black diamonds represent measurements from fixed samples and gray circles represent measurements from live samples.

with fewer particles that had low OFSC/PFSC, than calcite particles (Supplementary data, Fig. S1A–C).

Chlorophyll-containing calcified *E. huxleyi* cells were clearly distinguished (by their high OFSC) from chlorophyll-containing non-calcified *E. huxleyi* cells even when co-occurring in the same sample (Fig. 3). Detached coccoliths were likewise readily distinguished from bacteria and non-cellular debris. The maximum

OFSC/PFSC of both calcified cells and detached coccoliths was always  $<1$ , consistent with depolarization rather than rotation of polarization of scattered light.

*Emiliana huxleyi* cells grown under low light show decreased calcification causing a decrease in SSC, although the effect of light limitation varies between strains (Van Bleijswijk *et al.*, 1994). Both cells and detached coccoliths grown under light levels ranging from 12.5 to 150  $\mu\text{mol photons m}^{-2} \text{s}^{-1}$  (Supplementary data, Fig. S2A) showed a modest decrease in SSC and a corresponding decrease in OFSC/PFSC at low light levels (12.5 and 21  $\mu\text{mol photons m}^{-2} \text{s}^{-1}$ ) compared with higher light levels (Fig. 4 and Supplementary data, Figs S3 and S4). Although cytometric signatures showed high repeatability among replicate cultures analyzed on different days, the change in calcification due to light levels implied by cytometric parameters was significant but small: NZEH cells appeared to remain relatively highly calcified under all light conditions tested.

The strength of the OFSC/PFSC signal (Figs 3 and 4) correlated well with qualitative microscopic observations (not shown): Cultures of strain NZEH always contained the highest proportion of calcified cells, which were completely covered with heavily calcified coccoliths. Cultures of the moderately calcifying strain 61-04-12 were found by microscopy and cytometry to contain a large proportion of non-calcified cells and the separation of calcified from non-calcified cells in the OFSC axis was more modest than in strain NZEH. Cultures of strain CCMP1516 contained almost no calcified cells detectable by microscopy, with the rare calcified cells carrying only one or two thin coccoliths (not shown). Likewise, cytometry detected a small number of cells showing a weakly increased OFSC signal, but these cells did not form a clearly distinct population. No detached coccoliths were found by microscopic examination in CCMP1516 cultures, but small particles showing a high OFSC/PFSC were seen by cytometry (Figs 3 and 4), which might represent detached fragments of incompletely formed coccoliths. Finally, the cytometric signature of completely non-calcified strain CCMP2090 was similar to that of de-calcified cells of strain NZEH.

Crushed chalk showed a much broader range of PFSC, SSC and OFSC/PFSC than detached *E. huxleyi* coccoliths (Fig. 4, Supplementary data, Fig. S5). Crushed chalk was found to contain a great diversity of coccoliths and fragments of coccoliths of different sizes (Supplementary data, Fig. S1D). The PFSC, SSC and OFSC/PFSC signatures of *E. huxleyi* coccoliths always fell within the range of that of crushed chalk.

To further explore how forward scatter and side scatter parameters vary with degree of calcification,

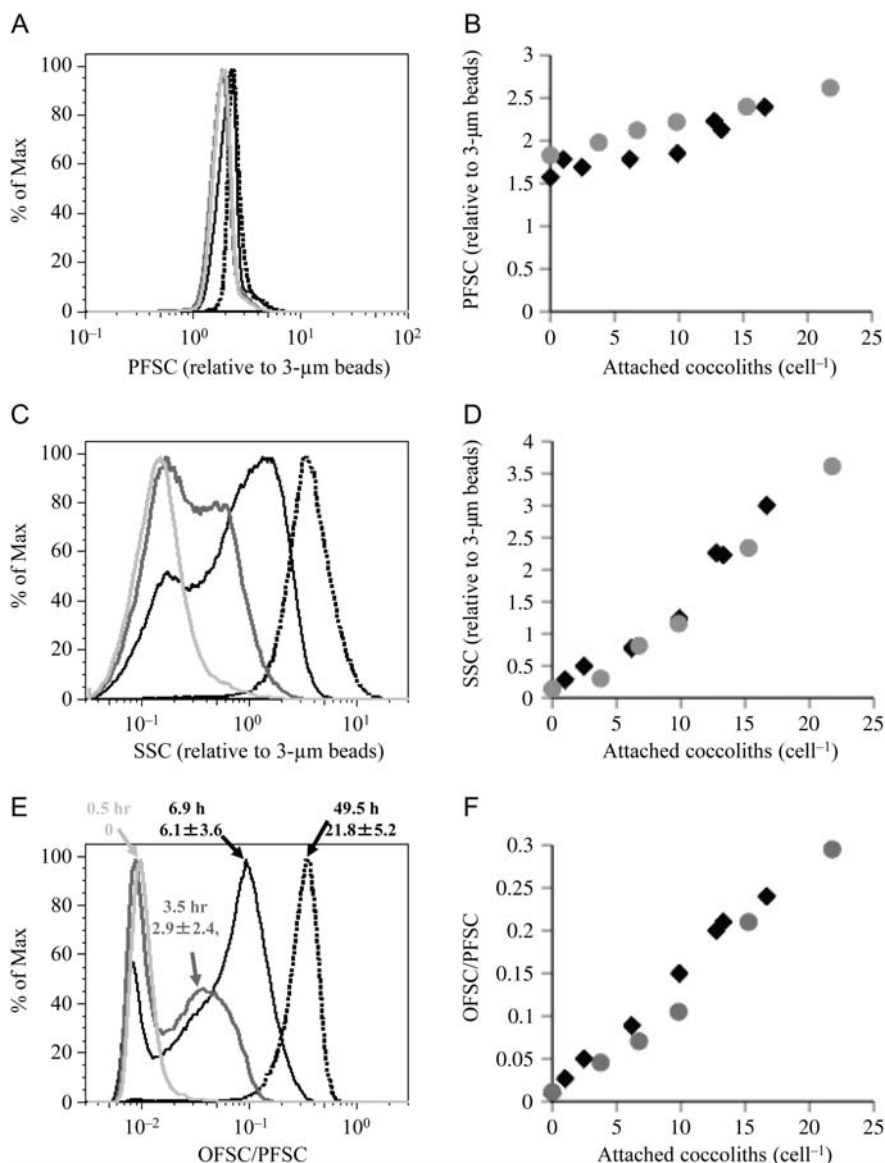


**Fig. 6.** Relationships between (A and B) PFSC, (C and D) SSC and (E and F) forward scatter polarization ratio OFSC/PFSC, SSC, and the number of attached coccoliths per cell. Representative histograms of PFSC (A), SSC (C) and OFSC/PFSC (E) for live cells analyzed at 0.5 h (light gray line), 3.5 h (dark gray line), 6.9 h (black line) and 49.5 h (dotted line) following restoration of pH after dissolution of coccoliths are shown. Numbers of attached coccoliths (mean  $\pm$  standard deviation) on calcified cells are indicated in (C). At time points when a substantial portion of chlorophyll-containing cells were not calcified, calcified and non-calcified sub-populations were discriminated and analyzed separately (in B, D, and F). Live cell measurements (in B, D, and F) represent the mean of adjacent time points taken within 1 h (Fig. 4). Error bars are not shown for clarity: the coefficients of variation between replicate fixed samples run on separate days was 3.1–5.6% (mean: 4.4%) for PFSC, 1.9–5.0% (mean: 3.7%) for SSC and 0.4–7.3% (mean: 3.6%) for OFSC/PFSC. The coefficients of variation for OFSC/PFSC between paired live samples taken within 1 h decreased with time from 11.4% at 3–4 h to 1.8% at 49–50 h. The averaged geometric coefficients of variation (used as populations displayed approximately log-normal distributions) for cytometric parameters of cell populations within samples was  $-20.5$  to  $+25.8\%$  (PFSC),  $-48.8$  to  $+98.0\%$  (SSC) and  $-40.9$  to  $+71.8\%$  (OFSC/PFSC).

strain NZEH was selected as it consistently exhibited close to 100% calcifying cells under a variety of growth conditions. Experiments were performed (i) de-calcifying cells and following the re-synthesis of coccoliths to test how OFSC/PFSC varied with the number of coccoliths per cell, and (ii) growing cells under a range of

extracellular  $[Ca^{2+}]$ , to test how OFSC/PFSC varied with the particulate Ca/coccolith.

NZEH cells grown in standard f/4-Si medium ( $[Ca^{2+}] \approx 9$  mM) were de-calcified by gradual addition of dilute HCl to acidify the medium (Fig. 5). Microscopic and cytometric observations showed that

*Table I: Linear regression analyses of relationships between light scatter parameters measured by flow cytometry (PFSC, SSC, OFSC/PFSC and SSC/PFSC, all normalized with respect to 3 μm calibration beads) and attached coccoliths cell<sup>-1</sup>*

	PFSC	SSC	OFSC/PFSC	SSC/PFSC
Fold change between min/max	1.66	26.0	32.7	18.2
Slope	$(4.11 \pm 0.54) \times 10^{-2}$	$(1.64 \pm 0.10) \times 10^{-1}$	$(1.37 \pm 0.07) \times 10^{-2}$	$(6.48 \pm 0.43) \times 10^{-2}$
$R^2$	0.831	0.957	0.970	0.949
$F_{(1,12)}$	58.8	265	392	223
Significance ( $P$ )	<0.0001	<0.0001	<0.0001	<0.0001
Deviation from linearity	No	No	No	No

In all cases, the slopes were not significantly different between fixed and live cells, so the data were pooled for regression analysis.

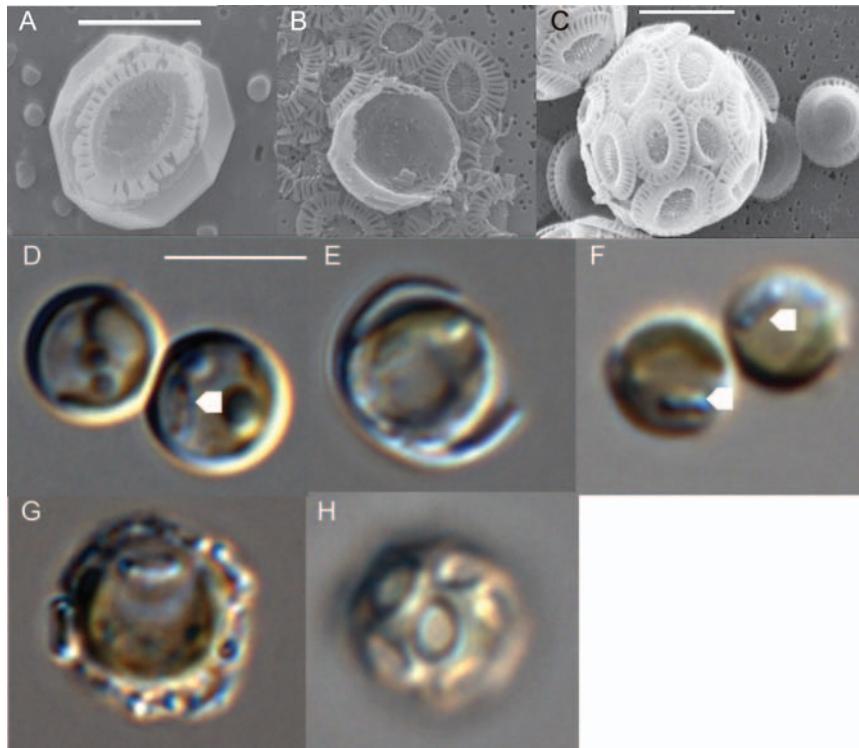


**Fig. 7.** Micrographs of *E. huxleyi* cells grown under varying extracellular [CaCl<sub>2</sub>]. **(A)** SEM image of a highly disintegrated coccolith found in culture grown in 0.3 mM CaCl<sub>2</sub>. Scale bar = 2 μm. **(B)** SEM image of a cell grown in 1 mM CaCl<sub>2</sub>. The coccosphere on this cell has collapsed, permitting the partially calcified coccoliths to be viewed in both sides. The thin organic casing of the cell is seen. **(C)** SEM image of a coccosphere grown in 10.5 mM CaCl<sub>2</sub>. Note the heavily calcified coccoliths. Scale bar for B and C = 3 μm. **(D)** Light micrograph of live cells grown in 0.1 mM CaCl<sub>2</sub>. Note the forming coccolith inside the cell on the right (arrowhead) and the presence of a refractive organic layer around the protoplast. **(E)** Light micrograph of a fixed cell grown in 0.3 mM CaCl<sub>2</sub>. Note that the organic layer has cracked and peeled away, revealing that it is separate from the underlying protoplasm. **(F)** Light micrograph of cells grown in normal seawater medium, 2.5 h after coccoliths were dissolved by temporarily dropping the pH to 6 and then restoring pH to 8.1. Note forming coccoliths inside both cells (arrowheads), and that the thick organic layer present on cells grown in low [Ca<sup>2+</sup>] media is not readily visible in this or in any other focal plane (not shown). **(G)** Cell grown under 0.3 mM CaCl<sub>2</sub> with partially formed, poorly calcified coccosphere. Focal plane in the middle of the cell to reveal a coccolith clearly forming in the interior of the cell. **(H)** Cell grown under 0.6 mM CaCl<sub>2</sub>, focal plane at the top of the cell to show that a complete coccosphere has been formed.

all attached and detached coccoliths were rapidly dissolved when the pH reached 6.0. Coincident with dissolution of coccoliths, the PFSC, SSC and OFSC/PFSC decreased. When the pH was restored (to 8.1) by addition of dilute NaOH, cells immediately began to

re-synthesize coccoliths that were secreted individually onto the cell surface. An average of 0.85 coccoliths were added per hour during the first 12 h, after which the rate slowed considerably as coccospheres carried one complete layer of coccoliths and coccolith production

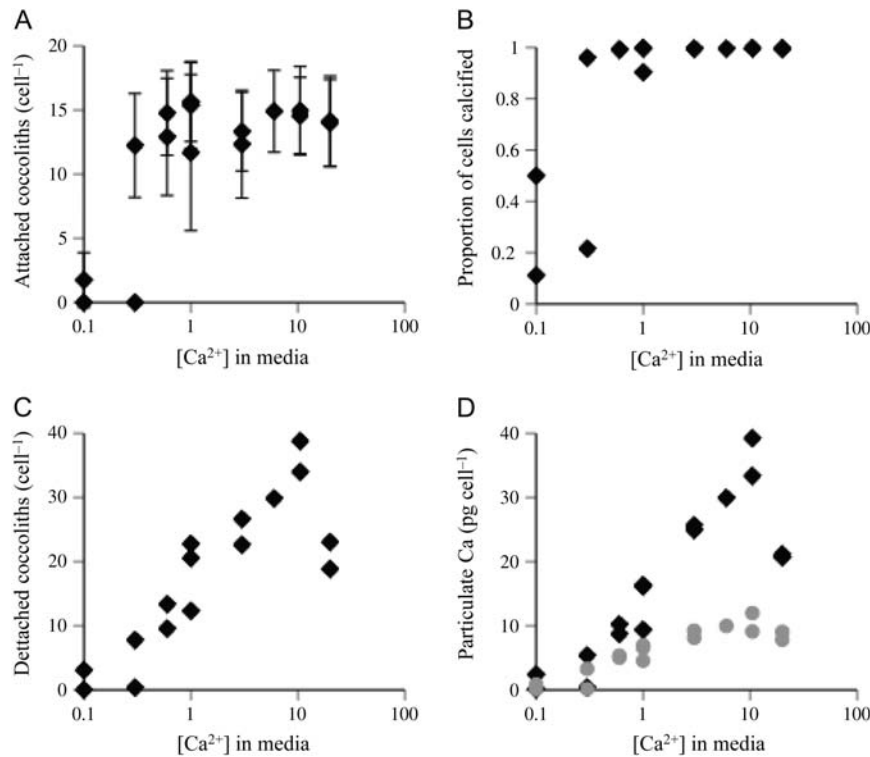


**Fig. 8.** Calcification states of *E. huxleyi* cultures grown under varying extracellular  $[CaCl_2]$ . **(A)** Number of attached coccoliths per cell. **(B)** Proportion of cells calcified. **(C)** Detached coccoliths present in media per cell. **(D)** Particulate Ca measured in the media, including cells and detached coccoliths (black diamonds), and the particulate Ca that can be attributed to cells (gray circles), accounting for the ratio of detached to attached coccoliths. For clarity, error bars are not shown in (B–D). Each point represents a single culture. Coefficients of variation for technical replicates of particulate Ca ranged from 0.0 to 13.3% (average 3.0%) and varied inversely with the total particulate Ca.

was balanced by cell division and detachment of coccoliths (Fig. 5A). PFSC, SSC and OFSC increased with the number of coccoliths added to the coccosphere. The increase in SSC and OFSC was much larger than the increase in PFSC. The SSC and the OFSC/PFSC ratio both exhibited a strong linear relationship with the number of coccoliths per cell (Fig. 6, Table I).

Notably, the cytometric properties of cultures were well maintained by fixation. SSC did not change upon fixation. PFSC did decrease by  $\sim 20\%$  in fixed compared with live cells, but this was a minor change considering that this parameter is generally measured (as here) on a log scale. As seen by the increase in detached coccoliths in fixed versus live cells (Fig. 5C), fixation did lead to the release of some coccoliths loosely attached in secondary layers on complete coccospheres, and this resulted in a somewhat higher OFSC/PFSC ratio of live cells at the latest time point selected. However, these effects of fixation were relatively minor and did not obscure general relationships. Therefore, for the remainder of the study, we focused on the analysis of fixed cells.

The calcification state of NZEH cells was then manipulated by culturing in artificial seawater with

varying  $[Ca^{2+}]$ . When grown in extracellular  $[Ca^{2+}] \leq 0.3$  mM, forming coccoliths could be seen inside many cells, but extracellular coccoliths on the cell surface or detached coccoliths showed very pronounced dissolution (Fig. 7). At these low concentrations of  $[Ca^{2+}]$ , cells carried only one or a few recently secreted coccoliths but never with a complete coccosphere. At extracellular  $[Ca^{2+}] \geq 0.6$  mM, the majority of cells were encased in complete coccospheres and the number of coccoliths per cell did not vary with extracellular  $[Ca^{2+}]$  (Figs 7 and 8A), with an average of  $14.1 \pm 3.8$  coccoliths  $cell^{-1}$  (Fig. 8A). Coccoliths became increasingly heavily calcified as extracellular  $[Ca^{2+}]$  increased, with heavily calcified coccoliths, typical of the R-morphotype, occurring at  $[Ca^{2+}] \geq 6$  mM (Fig. 7). The total concentration of particulate calcite (PCa) per cell (including detached coccoliths) increased over 10-fold with  $[Ca^{2+}]$  in the media between 0.3 and 10.5 mM (Fig. 8). Part of the increase in PCa was due to the increased production of detached coccoliths. However, the amount of calcite calculated to be physically associated with coccospheres was also increased strongly with the concentration of extracellular  $[Ca^{2+}]$ .

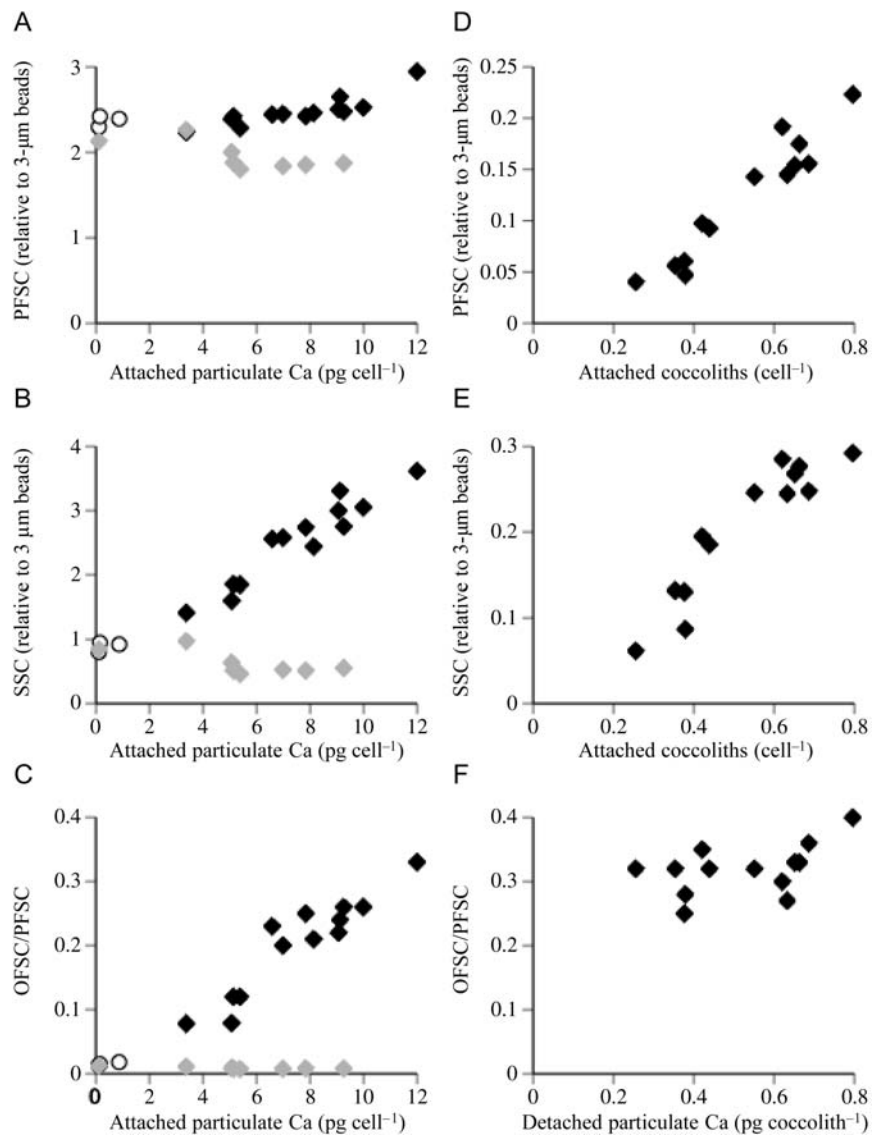


**Fig. 9.** (A–C) Flow cytometric light scattering parameters in relationship to the attached particulate Ca per cell. (A) PFSC. (B) SSC. (C) Forward scatter polarization ratio OFSC/PFSC. Black diamonds represent populations of cells with a complete coccosphere. (D) Forward scatter polarization ratio OFSC/PFSC of detached coccoliths versus the mass of calcite per coccolith. (A–D) Gray circles represent cells after acidification to dissolve coccoliths. White circles represent samples where the average cell contained less than one complete coccosphere. Each point represents a single culture. Error bars not shown (as in previous figures).

*Table II: Linear regression analyses of relationships between light scatter parameters measured by flow cytometry (PFSC, SSC, OFSC/PFSC and SSC/PFSC, all normalized with respect to 3 μm calibration beads) and attached Ca (pg cell<sup>-1</sup>)*

	PFSC	SSC	OFSC/PFSC	SSC/PFSC
Fold change between min/max	1.33	4.51	25.4	3.58
Slope	$(3.24 \pm 0.89) \times 10^{-2}$	$(2.41 \pm 0.15) \times 10^{-1}$	$(2.73 \pm 0.19) \times 10^{-2}$	$8.59 \pm 0.60) \times 10^{-2}$
$R^2$	0.484	0.951	0.935	0.936
$F_{(1,14)}$	13.1	270	203	205
Significance ( $P$ )	0.0028	<0.0001	<0.0001	<0.0001
Deviation from linearity	No	No	No	No

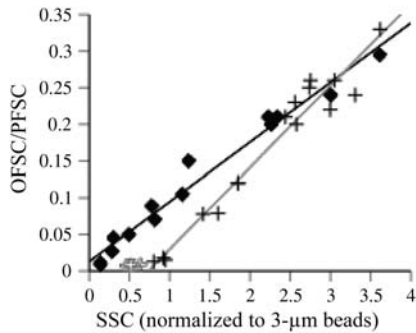


**Fig. 10.** Relationship between OFSC/PFSC and SSC when the number of coccoliths per coccospere was varied (black diamonds) and when the degree of calcification of coccoliths was varied by changing extracellular  $[\text{CaCl}_2]$  (simple cross symbols represent complete coccospere, open cross symbols represent cells with less than a complete coccospere). Error bars not shown (as in previous figures).

Extracellular  $[\text{Ca}^{2+}]$  did not have a significant effect on growth rate over the concentration ranges tested ( $0.1\text{--}20\text{ mM } [\text{CaCl}_2]$ ,  $\mu = 0.97 \pm 0.15\text{ day}^{-1}$  averaged over all concentrations, slope of  $\mu$  versus  $[\text{CaCl}_2] = 6.04 \times 10^{-3}$ , not different from 0,  $P = 0.33$ , see Supplementary data, Fig. S2B), as found in previous studies (Trimborn *et al.*, 2007).

PFSC, SSC and OFSC/PFSC all showed strong linear relationships with the amount of calcite attached to the cell, and SSC and OFSC/PFSC were much more strongly affected than PFSC (Fig. 9A–C and Table II). PFSC and SSC displayed strong linear relationships with particulate Ca mass (Fig. 9D and E), but no significant relationship was found between the OFSC/PFSC of detached coccoliths and their particulate Ca mass (Fig. 9F). Rapid and complete dissolution of attached coccoliths by acid treatment decreased PFSC, SSC and OFSC/PFSC to low levels, and PFSC, SSC and OFSC/PFSC did not decrease when non-calcified cells (grown in low extracellular  $[\text{Ca}^{2+}]$ ) were acidified. However, acid-treatment reduced SSC and OFSC/PFSC of calcified cells to levels lower than the levels of cells that were poorly or non-calcified due to growth in extracellular  $[\text{Ca}^{2+}] \leq 0.3\text{ }\mu\text{M}$  (Fig. 9B and C, Supplementary data, Fig. S7C).

Cells grown in low  $[\text{Ca}^{2+}]$  media had a thick organic coating. In transmitted light microscopy at high power, this coating could be distinguished as a refractive layer using Nomarski optics, but was most evident after fixation, where it occasionally fractured, causing it to separate from the protoplast. This coating was also observed in non-fixed cells that had been filtered and dried for scanning electron microscopy, and was even revealed under weakly calcified cells when the coccospere collapsed. The organic coating could not be

distinguished by transmitted light microscopy on cells grown in natural seawater; however, the coating was previously noted in transmission electron microscopy studies of calcifying and non-calcifying diploid cells of *E. huxleyi* (Klaveness and Paasche, 1971), so might be present on all cells but increased in thickness by growth in low  $[\text{Ca}^{2+}]$  media. In cells grown in media with  $\leq 0.3\text{ }\mu\text{M } [\text{Ca}^{2+}]$ , the thickness of this coating was estimated to be up to  $0.4\text{ }\mu\text{m}$  by measurements taken from light micrographs of cells from which the coating had been fractured away from the protoplast. The increased radius of non-calcifying cells due to the thicker organic covering might have accounted for the larger PFSC and SSC of cells grown in low  $[\text{Ca}^{2+}]$  compared with de-calcified cells grown in media with higher  $[\text{Ca}^{2+}]$ .

There were strong linear relationships between OFSC/PFSC and SSC (Fig. 10). However, the slope of the OFSC/PFSC to SSC relationship when the calcite per coccolith was varied ( $0.112$ ,  $R^2 = 0.956$ ,  $P < 0.0001$ , 95% confidence interval of slope:  $0.098\text{--}0.125$ ) was larger than that of this relationship when coccolith number was varied ( $0.081$ ,  $R^2 = 0.975$ ,  $P < 0.0001$ , 95% confidence interval:  $0.073\text{--}0.090$ ), and the slopes were judged to be significantly different ( $F_{1,26} = 17$ ,  $P = 0.00034$ ).

## DISCUSSION

The principal advantages of using forward scatter polarization to detect and measure the calcite content of coccolithophores are that it is highly specific, highly sensitive and requires no use of fluorescent dyes. As shown here and in previous studies, SSC also varies strongly with calcification state (Van Bleijswijk *et al.*, 1994), but SSC will also be high for pennate diatoms and will vary much more with the internal non-mineralized structures of cells, making it non-specific (Olson *et al.*, 1989). A few non-coccolithophore cells might display increased OFSC/PFSC signals, including certain cryptophytes (due to intracellular polarizing bodies) and calcified dinoflagellates such as *Thoracosphaera heimii* (Olson *et al.*, 1989). Cryptophytes are easily distinguished by phycoerythrin fluorescence (Olson *et al.*, 1989) and calcareous dinoflagellates are typically much less abundant than coccolithophores in water column samples (Gould and Fryxell, 1988; Hiramatsu and De Deckker, 1996; Karwath *et al.*, 2000b) and have a larger cell size (Karwath *et al.*, 2000a) than the most abundant smaller coccolithophores such as *E. huxleyi* or *Gephyrocapsa* species (so might be distinguished by FSC and chlorophyll fluorescence). However, in field applications, it would still be advisable to use microscopic examination

in parallel. Indeed, polarization-sensitive flow cytometers have already shown utility for separating calcified phytoplankton in field samples (Olson *et al.*, 1989; Balch *et al.*, 1999).

The present study provides two significant advances in the use of polarization-sensitive flow cytometry for studies of phytoplankton. First, our data suggest that the Brewster's Window analyzer used in this study is considerably more sensitive than methods using polarizing filters to separate the parallel and orthogonally polarized components of scattered or fluorescent light from analyzed cells, as employed in previous studies (Olson *et al.*, 1989; Balch *et al.*, 1999). The fully calcified cells of the coccolithophores *E. huxleyi* and *Hymenomonas carterae* (now *Pleurochrysis carterae*) compared by Olson *et al.* (Olson *et al.*, 1989) were reported to increase the ratio of orthogonally polarized to parallel polarized scattered light by only 2- to 3-fold relative to non-calcified cells of the same species. In comparison, the ratios observed in the present study obtained values over 40-fold greater for calcified *E. huxleyi* cells compared with non-calcified cells.

Second, our data indicate that the forward scatter polarization state exhibits linear relationships both with the number of coccoliths on the cell surface and with the degree of calcification of the coccoliths. In contrast to cells covered in coccospheres containing at least one complete layer of coccoliths, there was no discernable relationship between the calcium mass and forward scatter polarization of detached coccoliths. However, side scatter and both PFSC and OFSC showed an approximately linear relationship with calcium mass for unattached coccoliths. There was variation of side scatter and forward scatter of decalcified cells depending on  $[Ca^{2+}]$  in growth media (discussed later), but this variation was much less than that between treatments before decalcification (and protoplast diameter did not show variation; data not shown). Therefore, to a first approximation, depolarization of forward scatter appears that it might be determined largely by the ratio between calcite coccolith mass to the organic protoplast.

We caution that the relationship between forward light scatter and the degree of calcification appears to be non-linear at finer level analyses, particularly with respect to detached coccoliths. The much higher spread in the SSC and OFSC/PFSC signatures of crushed chalk compared with detached *E. huxleyi* coccoliths suggests that coccoliths of other species and coccolith fragments have signatures distinct from *E. huxleyi* coccoliths. Although OFSC/PFSC surprisingly did not vary consistently with Ca mass of individual coccoliths when extracellular  $[Ca^{2+}]$  was varied, coccolith OFSC/PFSC did vary modestly (max  $\approx 20\%$ ) between cells grown under low light and high light.

Light scatter from individual coccoliths is complex and highly orientation-dependent (Gordon *et al.*, 2009). Thus, even randomly oriented detached coccoliths may exhibit complex scatter signals in flow cytometry, as has been seen, for example, in mammalian erythrocytes (Van den Engh and Visser, 1979). The different angular orientations of coccoliths relative to the laser likely strongly influence light scatter (Supplementary data, Fig. S8). The laser will be incident on the proximal shield (concave) of some coccoliths, the distal shield (concave) of others and exactly on the rim for a more narrow range of angular orientations. Before injection into the sheath fluid, sample fluid passes through a capillary line experiencing Poiseuille (tube) flow with a parabolic velocity profile. In this tube flow, disks (a shape close to that of a coccolith) will adopt preferential orientations with the disk facing perpendicular to the plane formed by the long axis of the flow and the disk center of mass and are likely to be preferentially located not along the flow center-line but distributed radially at an intermediate distance between the sample line wall and the center line (Jeffery, 1922; Karnis *et al.*, 1966; Qi *et al.*, 2002; Pan *et al.*, 2008). Preferential orientations of coccoliths might be preserved upon injection into the sheath flow (Lucas and Pinkel, 1986) (Supplementary data, Fig. S9), and could cause further structure in the scatter signature from detached coccoliths. Indeed, detached coccoliths from normally or highly calcified cells displayed multi-modal relationships of light scatter parameters in 2D histograms (Supplementary data, Fig. S10).

There is no evidence that the complex optical signatures of detached coccoliths represent real population heterogeneity, and we suspect that they reflect instead the strong optical anisotropy of individual coccoliths and possible preferential orientations of populations of detached coccoliths as they pass through the laser. Coccoliths formed by exponentially growing cells (as tested here) may show standard deviations  $\approx 10\%$  in distal shield length, width and length of the central area and number of segments forming the coccoliths (Young and Westbrook, 1991), variations likely to have normal distributions. Small proportions of malformed coccoliths may be excreted (Young and Westbrook, 1991), but our SEM observations did not reveal these under moderate to high calcifying conditions. Indeed, the multi-modal (or sometimes donut-shaped) signature of detached coccoliths in scatter parameters only disappeared for the small and highly heterogeneous populations of incomplete coccoliths found in cultures grown at 0.3 mM  $[CaCl_2]$  (Supplementary data, Fig. S10), where elements beyond the protococcolith ring, the first structure formed in coccolithogenesis (Young *et al.*, 1999), were

incompletely formed (see example in Fig. 7). In contrast, the multi-modal signature was present even for lightly calcified, but complete detached coccoliths produced in cultures grown at 0.6 mM  $[\text{CaCl}_2]$  (Supplementary data, Fig. S10). One of us (P.D.) has observed that detached coccoliths occurring in exponentially growing cultures of several other strains (including axenic strains) under distinct growth conditions also exhibit bimodal SSC signatures when analyzed by other flow cytometers (the FACS Canto II, FACS Calibur and FACS Sort cytometers; unpublished data not shown), so the complex scatter signature is unlikely to be a result peculiar to the strains/conditions tested in this study or to the Influx cytometer used.

It is well beyond the scope of this study to attempt to quantitatively relate optical signatures to specific orientations of individual coccoliths, but we mention these considerations to explain qualitatively why even homogeneous populations of coccoliths produced by healthy, exponentially growing cells may exhibit a complex signature in PFSC, SSC and OFSC/PFSC. Specially designed fluidics (e.g. Johnson and Pinkel, 1986) might permit sufficient control of detached coccolith orientations to make use of this effect for future investigation of the optical properties of detached coccoliths.

Side scatter light also showed linear relationships both with the number of coccoliths on the cell surface and with the degree of calcification of the coccoliths. Side scatter has previously been reported to show a positive linear relationship with the square-root of calcite content of coccospheres for type A but not for multi-layer coccospheres of type B *E. huxleyi* cells (Van Bleijswijk *et al.*, 1994). The reasons for the differences in the relationship between side scatter and calcite content found in this study and in the study by Van Bleijswijk *et al.* (van bleijswijk *et al.*, 1994) might be due to (i) the different configuration of the side scatter optics employed, and (ii) the fact that the earlier study (Van Bleijswijk *et al.*, 1994) did not separate the contribution of attached versus unattached coccoliths to particulate calcite. Coccospheres carrying more than 1.5–2 layers of coccoliths were not observed in the strain NZEH. In other strains that we examined, the occurrence of cells with >2 layers of coccospheres was observed in late exponential and stationary phase cultures (data not shown), but in such cultures, the distribution of coccolith number per coccosphere was very broad, so they were not selected for experiments. We cannot yet rule out that the relationships between side scatter, forward scatter polarization and calcite content might become non-linear as coccospheres become covered in >2 layers of coccoliths. However, our limited data for coccospheres with >1 layer of coccoliths ( $\approx 12$  coccoliths per cell) showed the same linear

relationship between forward scatter depolarization and coccolith number as that observed for incomplete coccospheres.

The relationship between side scatter light and forward scatter light depolarization differed depending on whether the number or the mass of coccoliths was varied. This observation might be partly explained by the fact that cells grown in extracellular  $[\text{CaCl}_2] < 1$  mM were often observed to form an acid-resistant organic outer casing and/or to exhibit amorphous material on the cell surface, which might reflect secretion of coccolith-associated polysaccharides or other organic material on the cell surface (De Jong *et al.*, 1979; Godoi *et al.*, 2009) that increased side scatter. This material may have some optical activity: The OFSC/PFSC of cells grown in 0.1 or 0.3 mM  $[\text{CaCl}_2]$  that did not form coccoliths did not change with acidification but was consistently slightly higher ( $\approx 27\%$ ) than the OFSC/PFSC of decalcified cells grown at higher  $[\text{CaCl}_2]$ , even though also quite low. However, the effect of this organic casing on forward scatter depolarization appeared smaller than on side scatter. The relationships between forward scatter polarization state and side scatter might permit partial coccospheres to be distinguished from those from which coccoliths have been detached and partial coccospheres resulting from failure to form normal coccoliths.

In conclusion, polarization-sensitive flow cytometry provides a method for rapidly assessing the calcification state of individual phytoplankton cells. It might be possible to make at least semi-quantitative comparisons between natural environmental samples run on different instruments with similar configurations, using calcite particles (from coccolith-rich chalk or crushed calcite crystal) as highly optically active standards. Advanced flow cytometers with this capacity have recently become commercially available and are now routinely used in many marine institutes. Although the technique described here does not directly allow the determination of calcification rates, it should permit the high-throughput quantitative or semi-quantitative comparison of the dynamics of calcified phytoplankton and their degree of calcification. An additionally important advantage of flow cytometric over microscopic techniques is the ability to sort cells based on their calcification properties.

## SUPPLEMENTARY DATA

Supplementary data can be found online at <http://plankt.oxfordjournals.org>.

## ACKNOWLEDGEMENTS

We graciously thank Dr Armbrust for access to laboratory space, culture facilities, microscopes and an InFlux flow cytometer during the major portion of studies reported here. We also thank Darryl Green for assisting with PIC analysis and Bob Head for assisting with POC analysis. The careful comments of two anonymous reviewers greatly improved the manuscript.

## FUNDING

P.D. was supported in part by an NSF Microbiology Post-doctoral Fellowship and by FONDECYT grant 1110575 during this study.

## CONFLICT OF INTEREST

G.E. is an employee of BD Biosciences, which sells the InFlux cytometer used in this study. Neither the lead author P.D. nor any of the other authors have any financial interests with BD Bioscience or the sale of InFlux instruments.

## REFERENCES

- Armstrong, R. A., Lee, C., Hedges, J. I. *et al.* (2001) A new, mechanistic model for organic carbon fluxes in the ocean based on the quantitative association of POC with ballast minerals. *Deep-Sea Res. Part II Top. Stud. Oceanogr.*, **49**, 219–236.
- Balch, W. M., Drapeau, D. T., Cucci, T. L. *et al.* (1999) Optical backscattering by calcifying algae: separating the contribution of particulate inorganic and organic carbon fractions. *J. Geophys. Res.*, **104**, 1541–1558.
- Balch, W. M., Drapeau, D. T., Fritz, J. J. *et al.* (2001) Optical backscattering in the Arabian Sea, a continuous underway measurements of particulate inorganic and organic carbon. *Deep-Sea Res. Part I: Oceanogr. Res. Papers*, **48**, 2423–2452.
- Beaufort, L., Couapel, M., Buchet, N. *et al.* (2008) Calcite production by coccolithophores in the south east Pacific Ocean. *Biogeosciences*, **5**, 1101–1117.
- Beaufort, L., Probert, I., De Garidel-Thoron, T. *et al.* (2011) Sensitivity of coccolithophores to carbonate chemistry and ocean acidification. *Nature*, **476**, 80–83.
- Berry, L., Taylor, A. R., Lucken, U. *et al.* (2002) Calcification and inorganic carbon acquisition in coccolithophores. *Funct. Plant Biol.*, **29**, 289–299.
- De Jong, E., Van Rens, L., Westbroek, P. *et al.* (1979) Biocalcification by the marine alga *Emiliania huxleyi* (Lohmann) Kamptner. *Eur. J. Biochem.*, **99**, 559–567.
- Ehrhardt, M. and Koeve, W. (2007) Determination of particulate organic carbon and nitrogen. *Methods of Seawater Analysis*. Wiley-VCH Verlag GmbH, Weinheim, Germany, pp. 437–444.
- Feely, R. A., Sabine, C. L., Lee, K. *et al.* (2004) Impact of anthropogenic CO<sub>2</sub> on the CaCO<sub>3</sub> system in the oceans. *Science*, **305**, 362–366.
- Feng, Y., Warner, M. E., Zhang, Y. *et al.* (2008) Interactive effects of increased pCO<sub>2</sub>, temperature and irradiance on the marine coccolithophore *Emiliania huxleyi* (Prymnesiophyceae). *Eur. J. Phycol.*, **43**, 87–98.
- Feng, Y. Y., Hare, C. E., Leblanc, K. *et al.* (2009) Effects of increased pCO<sub>2</sub> and temperature on the North Atlantic spring bloom. I. The phytoplankton community and biogeochemical response. *Mar. Ecol. Prog. Ser.*, **388**, 13–25.
- Frankignoulle, M., Canon, C. and Gattuso, J. P. (1994) Marine calcification as a source of carbon dioxide: positive feedback of increasing atmospheric CO<sub>2</sub>. *Limnol. Oceanogr.*, **39**, 458–462.
- Godoi, R. H. M., Aerts, K., Harlay, J. *et al.* (2009) Organic surface coating on coccolithophores—*Emiliania huxleyi*: its determination and implication in the marine carbon cycle. *Microchem. J.*, **91**, 266–271.
- Gordon, H. R., Smyth, T. J., Balch, W. M. *et al.* (2009) Light scattering by coccoliths detached from *Emiliania huxleyi*. *Appl. Optics*, **48**, 6059–6073.
- Gould, R. W. and Fryxell, G. A. (1988) Phytoplankton species composition and abundance in a Gulf Stream warm core ring. I. Changes over a five month period. *J. Mar. Res.*, **46**, 367–398.
- Hiramatsu, C. and De Deckker, P. (1996) Distribution of calcareous nanoplankton near the Subtropical Convergence, south of Tasmania, Australia. *Mar. Freshwater Res.*, **47**, 707–713.
- Iglesias-Rodriguez, M. D., Halloran, P. R., Rickaby, R. E. M. *et al.* (2008) Phytoplankton calcification in a high-CO<sub>2</sub> world. *Science*, **320**, 336–340.
- Jeffery, G. B. (1922) The motion of ellipsoidal particles immersed in a viscous fluid. *Proc. Roy. Soc. London. Ser. A, Contain. Papers Math. Phys. Char.*, **102**, 161–179.
- Johnson, L. A. and Pinkel, D. (1986) Modification of a laser-based flow cytometer for high-resolution DNA analysis of mammalian spermatozoa. *Cytometry*, **7**, 268–273.
- Karnis, A., Goldsmith, H. L. and Mason, S. G. (1966) The flow of suspensions through tubes: V. Inertial effects. *Can. J. Chem. Eng.*, **44**, 181–193.
- Karwath, B., Janofske, D., Tietjen, F. *et al.* (2000a) Temperature effects on growth and cell size in the marine calcareous dinoflagellate *Thoracosphaera heimii*. *Mar. Micropaleontol.*, **39**, 43–51.
- Karwath, B., Janofske, D. and Willems, H. (2000b) Spatial distribution of the calcareous dinoflagellate *Thoracosphaera heimii* in the upper water column of the tropical and equatorial Atlantic. *Int. J. Earth Sci.*, **88**, 668–679.
- Klavness, D. and Paasche, E. (1971) Two different *Coccolithus huxleyi* cell types incapable of coccolith formation. *Arch. Fur Mikrobiol.*, **75**, 382–385.
- Lakhtakia, A. (1989) Would Brewster recognize today's Brewster angle? *Optics News*, **15**, 14–18.
- Langer, G., Geisen, M., Baumann, K. H. *et al.* (2006) Species-specific responses of calcifying algae to changing seawater carbonate chemistry. *Geochem. Geophys. Geosyst.*, **7**, Q09006.
- Langer, G., Nehrke, G., Probert, I. *et al.* (2009) Strain-specific responses of *Emiliania huxleyi* to changing seawater carbonate chemistry. *Biogeosciences*, **6**, 2637–2646.

- Lucas, J. N. and Pinkel, D. (1986) Orientation measurements of microsphere doublets and metaphase chromosomes in flow. *Cytometry*, **7**, 575–581.
- Morel, F. M. M., Rueter, J. G., Anderson, D. M. *et al.* (1979) Aquil: a chemically defined phytoplankton culture medium for trace metal studies. *J. Phycol.*, **15**, 135–141.
- Olson, R. J., Zettler, E. R. and Anderson, O. K. (1989) Discrimination of eukaryotic phytoplankton cell-types from light scatter and autofluorescence properties measured by flow-cytometry. *Cytometry*, **10**, 636–643.
- Paasche, E. (2001) A review of the coccolithophorid *Emiliania huxleyi* (Prymnesiophyceae), with particular reference to growth, coccolith formation, and calcification-photosynthesis interactions. *Phycologia*, **40**, 503–529.
- Pan, T.-W., Chang, C.-C. and Glowinski, R. (2008) On the motion of a neutrally buoyant ellipsoid in a three-dimensional Poiseuille flow. *Comput. Methods Appl. Mech. Eng.*, **197**, 2198–2209.
- Qi, D., Luo, L., Aravamuthan, R. *et al.* (2002) Lateral migration and orientation of elliptical particles in Poiseuille flows. *J. Stat. Phys.*, **107**, 101–120.
- Riebesell, U., Zondervan, I., Rost, B. *et al.* (2000) Reduced calcification of marine plankton in response to increased atmospheric CO<sub>2</sub>. *Nature*, **407**, 364–367.
- Trimborn, S., Langer, G. and Rost, B. (2007) Effect of varying calcium concentrations and light intensities on calcification and photosynthesis in *Emiliania huxleyi*. *Limnol. Oceanogr.*, **52**, 2285–2293.
- Van Bleijswijk, J. D. L., Kempers, R. S. and Veldhuis, M. J. (1994) Cell and growth characteristics of types A and B of *Emiliania huxleyi* (Prymnesiophyceae) as determined by flow cytometry and chemical analyses. *J. Phycol.*, **30**, 230–241.
- Van den Engh, G. J. and Visser, J. W. M. (1979) The light scattering properties of pluripotent and committed haemopoietic stem cells. *Acta Haematol.*, **62**, 289–298.
- Young, J. R., Davis, S. A., Bown, P. R. *et al.* (1999) Coccolith ultrastructure and biomineralisation. *J. Struct. Biol.*, **126**, 195–215.
- Young, J. R. and Westbroek, P. (1991) Genotypic variation in the coccolithophorid species *Emiliania huxleyi*. *Mar. Micropaleontol.*, **18**, 5–23.
- Ziveri, P., De Bernardi, B., Baumann, K. H. *et al.* (2007) Sinking of coccolith carbonate and potential contribution to organic carbon ballasting in the deep ocean. *Deep-Sea Res. Part II: Top. Stud. Oceanogr.*, **54**, 659–675.
- Zondervan, I. (2007) The effects of light, macronutrients, trace metals and CO<sub>2</sub> on the production of calcium carbonate and organic carbon in coccolithophores—a review. *Deep-Sea Res. Part II: Top. Stud. Oceanogr.*, **54**, 521–537.